Italian Association of Aeronautics and Astronautics
XXV International Congress
9-12 September 2019 | Rome, Italy

AERODYNAMIC CHARACTERISATION OF VEGA-C LAUNCHER

P.L. Vitagliano[1], F. De Gregorio[1*], P. Roncioni[1], F. Paglia[2], C. Milana[2]

[1]CIRA (Italian Aerospace Research Centre), via Maiorise, 81043 Capua (CE), Italy

[2]AVIO Spa, via Ariana km 5,2 – 00034 Colleferro (RM), Italy

*f.degregorio@cira.it

ABSTRACT

The aerodynamic characterization of the new Vega C space launcher has been carried out by CIRA in collaboration with AVIO. The aerodynamic database is an important input for the flight dynamics and the structural design. The Vega C behaviour has been studied through wind tunnel tests in the range of Mach 0.5 and 3.5 and through numerical simulations for the entire atmospheric flight envelope. A large test matrix was considered, covering four stages and three stages configurations, with and without protrusions, including plume, canted nozzle, wind tunnel sting and Reynolds number from flight to wind tunnel conditions. The paper describes the experimental and numerical activities, considering global aerodynamic coefficients and pressure distributions, together with flow visualizations.

Keywords: VEGA-C, Space Launcher, Aerodynamic, EXP/CFD characterization.

1 INTRODUCTION

In 1957, the Soviet Union launched Sputnik 1, the first artificial satellite, a sphere of 58 cm in diameter and weighing about 84 kg, equipped with four antennas and two radio transmitters. This event started the race for space exploration and its commercial and strategic exploitation. Since then, an enormous development has been achieved in many fields as communications, electronics, computing science, numerical simulation, environmental measurement techniques, sensors, image and spectral detection systems that has allowed the creation of ever more sophisticated and efficient satellites compared to the founder Sputnik 1. These allowed the creation of a worldwide telecommunications network, geo-navigation systems, earth monitoring systems, meteorological satellites and a great improvement in the scientific research of our planet and the space that surrounds us. All this has required and continues to require efficient and reliable transport systems for the launch of new satellites families or space vehicles.

In this context, the European Space Agency (ESA) offers a fleet of launch vehicles (LV): Ariane, Soyuz and Vega. Thanks to their complementarities, they cover all commercial and governmental missions' requirements, providing access to the different types of orbit from Low Earth Orbit (LEO) to Geostationary Transfer Orbit (GTO), and even to interplanetary destinations. The Vega solution complements the Ariane 5 and Soyuz offers for small to medium payloads, for Sun-Synchronous (SSO) and Low-Earth (LEO) Orbits. Vega is a four stages launcher vehicle (LV), operative since 2012. The Italian company AVIO is in charge of the Vega LV development and production.

Following the decisions taken during the December 2014 and December 2016 ESA Ministerial Councils, ESA and European industry are currently developing Vega C, an upgraded and more powerful version of Vega. The main objective is to increase the launcher performance and the flexibility for multiple payloads missions. The published user manuals ([1] and [2]) indicate a performance improvement of about 65% with respect to Vega.
The Vega C configuration foresees the development of a new and more powerful Solid Rocket Motor (SRM), named P120c, for the 1st stage, which will also be used as a strap-on booster for the Ariane 6-2 (2 boosters) and Ariane 6-4 (4 boosters) configurations. The 2nd stage is upgraded using the more powerful SRM Zefiro 40 (Z40). The 3rd stage SRM remains almost unchanged with the Z9 SRM. The 4th stage provides an improved AVUM+ with 30% more propellant. A new fairing allows the accommodation of larger and heavier pay loads (Figure 1).
The Vega evolution involves considerable differences in the external geometry. The main ones are larger first and second stages, new interstage components, larger payload fairing, different external protrusions both in terms of position and quantity. In Figure 2, Vega and Vega C geometries are superimposed to highlight the differences. These changes require an in-depth study of the launcher's new aerodynamics in order to guarantee the correct balance in terms of weight, thrust and aerodynamic forces, the absence of potentially destructive aerodynamic instability phenomena as the buffeting [3] and the correct structural design providing the distribution of aerodynamic loads on the various components of the launcher.

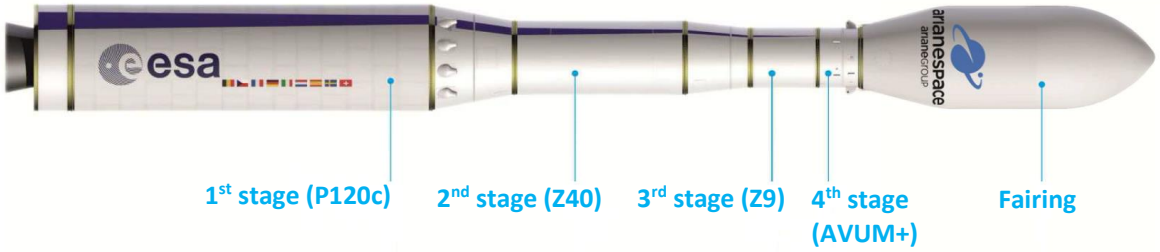

Figure 1: Vega C configuration, (figure 1.4.1 of Vega C user's manual [2] .

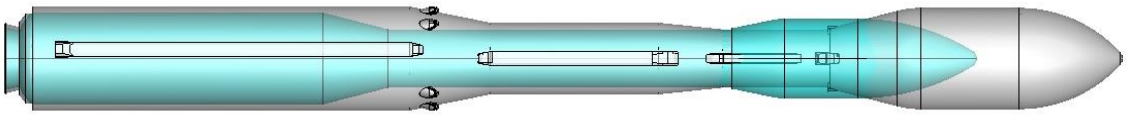

Figure 2: Vega C (grey colour) vs Vega (light blue colour) geometry.

CIRA and AVIO, in close collaboration, conducted a numerical / experimental investigation aimed at defining the launcher's aerodynamic behaviour in all its flight phases. The article deals with the numerical and experimental activities aimed to characterise the aerodynamic behaviour at different Mach and Reynolds number. A dedicated scaled model has been designed, manufactured and subsequently tested in the trisonic INCAS wind tunnel. The paper briefly describes the experimental and numerical activities and discuss part of the obtained results.

2 EXPERIMENTAL SET UP

The experimental test campaign was conducted at INCAS trisonic blowdown wind tunnel. The pressurised circuit and the test section sizes (1.2m x 1.2m) allow to reach high Reynolds number values. The facility operates in the Mach range between M=0.5 to M=3.5. Two test sections are available: one with solid walls for subsonic and supersonic speed regimes the second one with perforated walls for transonic flow. A complete description of the facility is reported in Munteanu [4]. A modular 1:30 scaled model was designed and manufactured in

order to withstand the severe aerodynamic conditions and allowing the investigation of multiple configurations. The model replicates, with and without the external protrusions, both the 3 stages and the 4 stages configurations.
The model was equipped with: a six-component strain gauge balance model TASK 2" (main features are summarised in Table 1), 57 pressure ports (PTS) distributed along two azimuth planes at ψ = 120° and ψ = 300° respectively (Figure 3) and an array of 24 dynamic pressure sensors along the plane at ψ = 0°.

	Fz [N]	Fy [N]	Fx [N]	Mx [Nm]	My [Nm]	Mz [Nm]
Full Scale	17800	17800	2670	339	1638	1356
Accuracy	35.6	35.6	5.34	0.678	3.276	2.712

Table 1: TASK 2 balance characteristics.

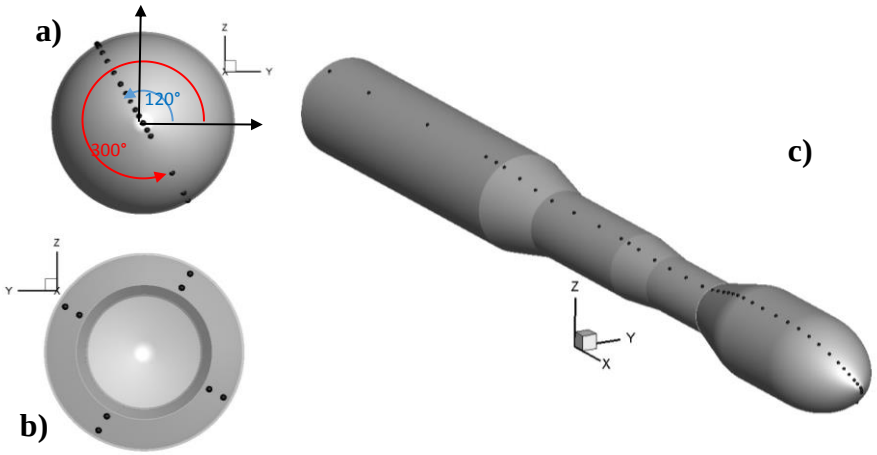

Figure 3: Pressure Ports location on model : a) front view, b) rear view, c) iso-view (right).

In the fairing, two Scaninvalve ZOC22B/32px pressure transducers with full scale range of ± 25 psi and ±50 psi respectively and accuracy of 0.02% of F.S. were installed and connected to the pressure ports. Furthermore, an electronic inclinometer was mounted in the fairing in order to evaluate possible model/sting deformation at high incidence angles and permits post processing data correction. Two accelerometers were installed on the fairing and on the launcher base to monitor the start and shutdown wind tunnel shocks. A motorised rear sting supported the model, allowing a sweep angle between α =-10° to α =10° with an accuracy of 0.1°.

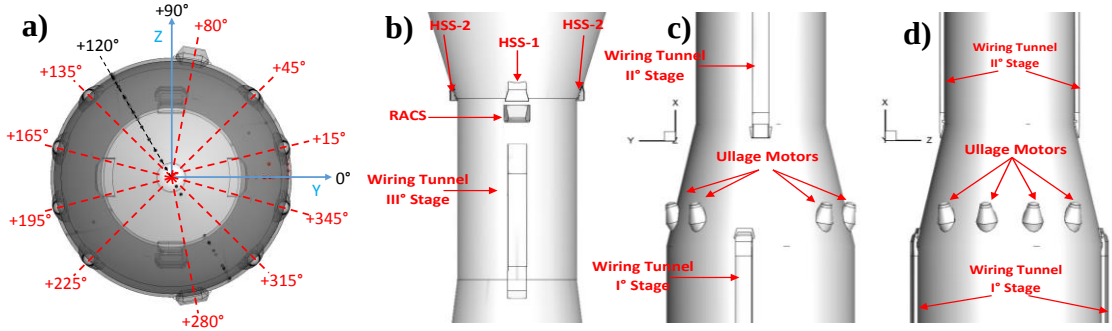

Figure 4: Protrusion description and positions: a) front view, b-c) top view, d) side view

On the model several protrusion were installed reproducing the shape of the following systems: four Horizontal Separation Systems (HSS) located on the 4th stage at ψ=0° and every 90°; two Roll and Attitude Control Systems (RACS) located just downstream of the "hammerhead", at

ψ =90° and ψ =270°; four wiring tunnels mounted on the 3rd and 2nd stage respectively at ψ =90° and ψ =270°; eight dummy fairings for the ullage motors on the 1/2 interstage at ψ =15°, 45°, 135°, 165°, 195°, 225°, 315° and 345°; and two wiring tunnels mounted on the 1st stage placed at ψ =80° and ψ=280°. Figure 4 provides an overview of the location of each protrusion on the model. Hereinafter, the clean model configuration is named as baseline, while the configuration with the external fairings installed is indicated as protrusion.

3 NUMERICAL SIMULATIONS

The objectives of the CFD activities were to produce a numerical data base of global and local aerodynamic coefficients [5], together with distributed loads, to cover the complete range of the launcher atmospheric flight and to allow for extrapolation of wind tunnel data to flight conditions. It is worth to note that wind tunnel measurements were carried out without engine plume, at low Reynolds number and limited Mach number range, and they did not provide information suitable to compute distributed loads. In particular, CFD results were required in the Mach number range above 3.5, since no data was available from the WT test.

A large test matrix was considered, covering 4 stages and three stages configurations, with and without protrusions, including plume, canted nozzle, wind tunnel sting and Reynolds number from flight to wind tunnel conditions.

Computations from subsonic to supersonic regimes were carried out using the multiblock structured flow solver ZEN, for steady and unsteady RANS equations, which has been developed at CIRA for more than two decades [6], [7]. It was used in the past for analysis of VEGA configuration both in flight and in wind tunnel conditions, demonstrating good agreement in the complete range of Mach and Reynolds numbers considered [8], [9]. Present results were obtained with k-ω TNT turbulence model.

Aerothermodynamic analysis in hypersonic range were carried out using the CIRA NExT code [10], that solves, on a multi-block structured grid, the RANS equations in a density-based approach.

Several computational grids were produced in order to perform the flow simulations: 4 stages clean configuration with nozzle and with wind tunnel sting for subsonic and transonic flows (free stream Mach from 0.5 to 1.2); 4 stages for supersonic flow (from M=1.7 to M=2.0), axi-symmetric, with 6 degrees canted nozzle and with wind tunnel sting; 4 stages for hypersonic flow (from M=3.5 to M=6.0) and 3 stages for hypersonic flow (from M=4.0 to M=7.0). Finally, a grid for complete 4 stages configuration with protrusions for transonic and supersonic flow. 17 different Mach numbers in the range between M=0.5 to M=7.0 were simulated, at three different angles of attack (α=0°, 5° and 10°) for 4 stages and 3 stages configurations.

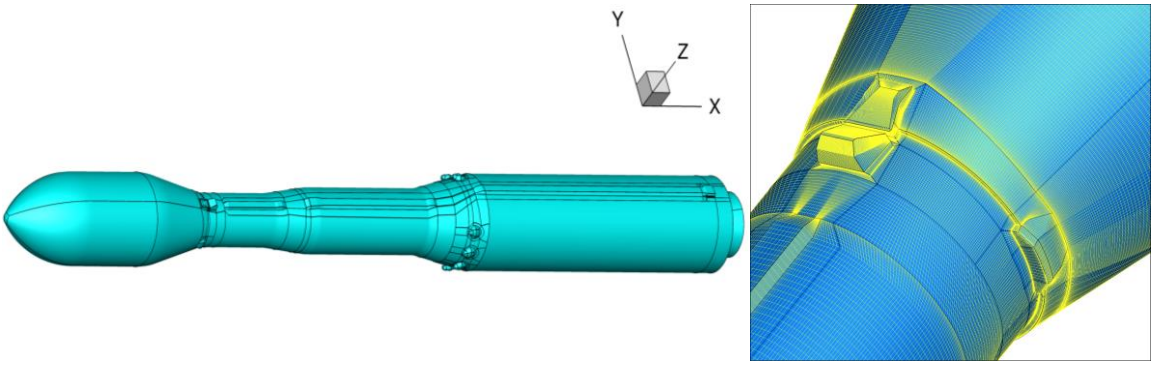

Figure 5: Complete configuration with protrusions. Left: Blocks boundaries on the surface. Right: Detail of the surface mesh in the boat-tail region.

Furthermore the effect of the canted nozzle thrust vectoring was examined in flight conditions at M=1.7 and M=2.0. Particular care was taken to examine the Reynolds effect by simulating the two wind tunnel Reynolds number conditions in addition to the flight Reynolds number and an intermediate value between the experiments and the flight condition. The 4 stages configuration with protrusion was investigated in WT and flight Reynolds conditions at fixed incidence angle of α=5° for different Mach (M=0.95, 1.8 and 5.0) and varying the roll angle.

4 WIND TUNNEL TEST PLAN

The experimental test campaign covered a variety of speed conditions from M=0.5 to M=3.5 investigating the 4 stages configuration with and without protrusions. Each WT run was carried out varying the model incidence angle in the range between α=-10° to α=10° in sweep mode with an angle resolution of 0.5 degree for the force and moment measurement and a better angle resolution of 0.1 degree for the pressure measurements. All runs were conducted to the maximum achievable Reynolds number ($Re=8x10^6$), except some ones (M=0.95, 1.05, 1.2, 1.8 and 2.0) that were also performed at the minimum Reynolds ($Re=2.5x10^6$) to be exploited for extrapolation to flight. Each polar was repeated varying the model roll angle, from ϕ=-30° to ϕ=150° with step of 30° in order to measure the pressure distribution on different azimuthal planes. Same procedure was used for the configuration with protrusions in order to evaluate the effect of the external fairings on the lateral stability.

5 RESULTS

The extensive numerical and experimental test campaign provided a complete aerodynamic database. The baseline configuration has been investigated varying Mach, Reynolds and incidence angle. The WT test allowed to investigate a limited range of Mach and Reynolds number with respect the flight envelope but provided the aerodynamic loads for the complete range of the incidence angle between α=-10° to 10° with a step of 0.5°. Figure 6 shows the experimental and numerical aerodynamic coefficients versus α, at M=0.95 and M=1.8 respectively. The diagrams show a good agreement between experiments and CFD for lift and pitching moment whereas larger difference occurs for CD. The reason is partly due to the malfunctioning of the balance and partly to the adopted correction procedure to remove the contribution from the base. This difference is taken into account by the accuracy of the aerodynamic database. Varying the flow speed from M=0.5 to M=1.2 the drag coefficient reaches a maximum value induced by the shock wave in front of the vehicle nose. By further increasing the free stream velocity (up to M=7), the drag coefficient shows a continuous reduction. Experimental and numerical results have the same trend even when the angle of attack varies. The experimental results show a negative shift with respect to the CFD due to the lack of the base contribution. Drag difference becomes negligible at M = 3.5, due to the reduction of the base pressure contribution with respect to the total drag.

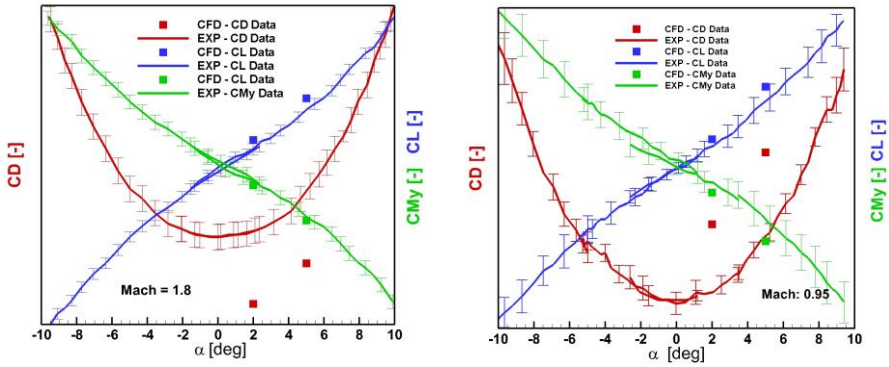

Figure 6: EXP and CFD forebody results: CD, CL and CMy behaviour versus α at Mach 0.95 and 1.8.

At α=5°, launcher lift coefficient increases up to M=2, and then it remains constant. The absolute value of the pitching moment shows a similar trend. At α=10°, the CL and CMy have a different behaviour with respect to α=5°, with the CL increasing up to M=3.5 and then decreasing, similar behavious shows the absolute value of the CMy. Both CL and CMy are characterised by a peak at sonic conditions (Figure 7).
The Reynolds effect presents a decrease of the drag and lift coefficient as the Reynolds number increases. Trend is confirmed by both experimental and numerical results (Figure 8). The pressure measurements provided a remarkable agreement with the CFD simulation confirming the reliability of the obtained results (Figure 9).

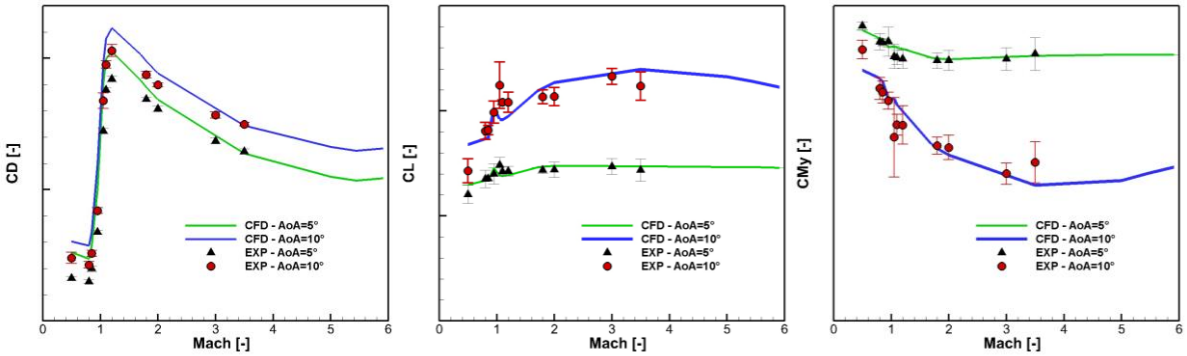

Figure 7: CD, CL and CMy versus Mach number for CFD and EXP respectively.

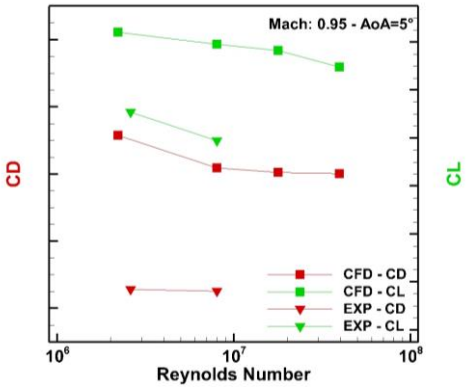

Figure 8: CD and CL versus Reynolds number at Mach 0.95 and α=5° for CFD and EXP data.

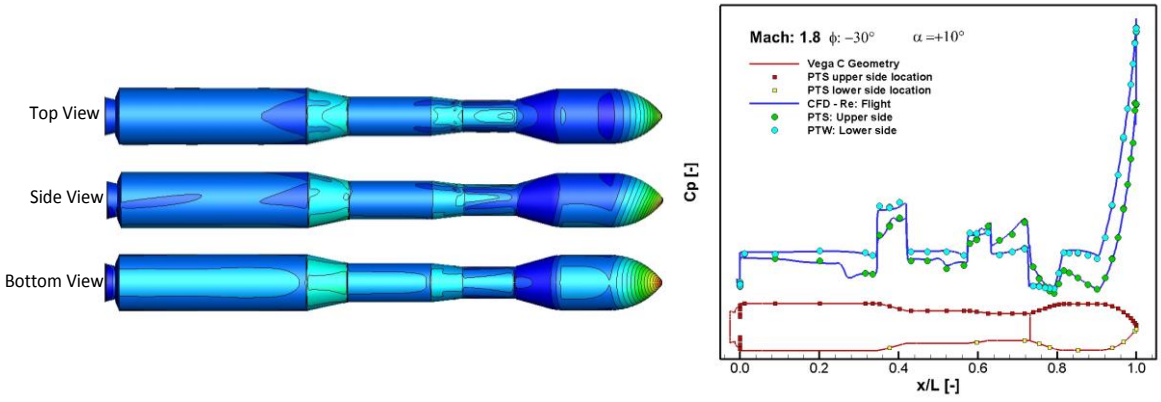

Figure 9: a) CFD Cp distribution colour maps, b) CFD & EXP Cp distribution comparison at Ψ=90°, Mach 1.8, α=10° and Re=8 x10^6 and flight respectively.

The numerical simulation provided a detailed description of the external flow field behaviour detecting the location of the shock wave and the detachment of the longitudinal vortices. At the same time, the oil flow visualization (Figure 10-a) results confirmed the goodness of the CFD

skin friction lines (Figure 10-b) showing similar flow pattern. Just the location of the boat tail vortex is slightly mismatched due to the different Reynolds number. The flight Reynolds CFD simulation locates the shock wave on the boat tail more downstream with respect to the oil flow image taken at Reynolds of $5x10^6$. Figure 10-c shows the external flow field in terms of iso-level of the Q-criterion surfaces. The iso-view and the cross planes clearly show the longitudinal vortex on the upper surface and the shock waves occurring on the boat tail and on the 2/3 and 1/2 interstages.

The contribution of the external fairings induces a substantial increment of the drag coefficient and almost negligible contribution on the lift and the pithing moment (Figure 11-a). Varying the roll angle, a clear effect of the protrusions on the rolling moment is observed. (Figure 11-b). The roll angle position induces positive and negative rolling moment depending on the relative position of the wiring tunnels.

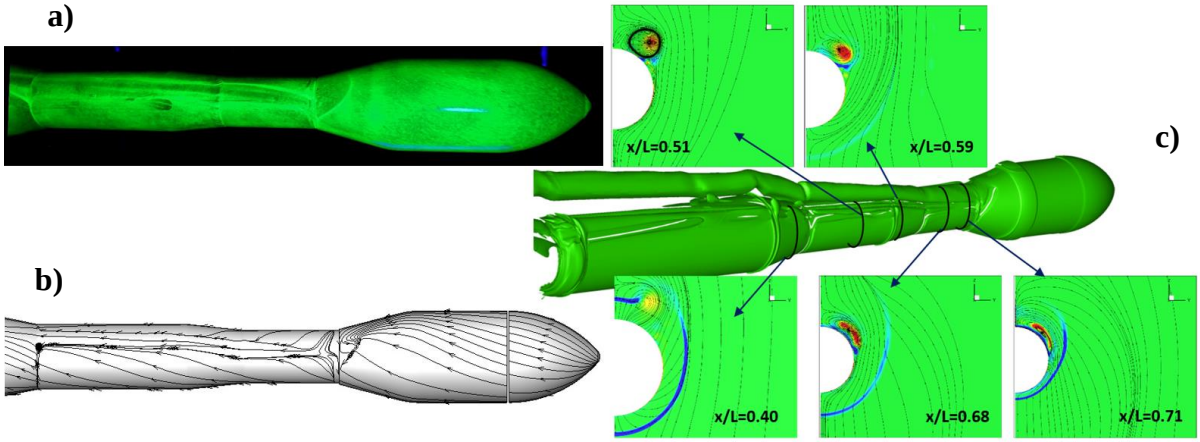

Figure 10: a) Oil flow visualization, b) CFD skin friction lines, c) Iso-level Q-criterion surface at Mach:1.8 and α=10°

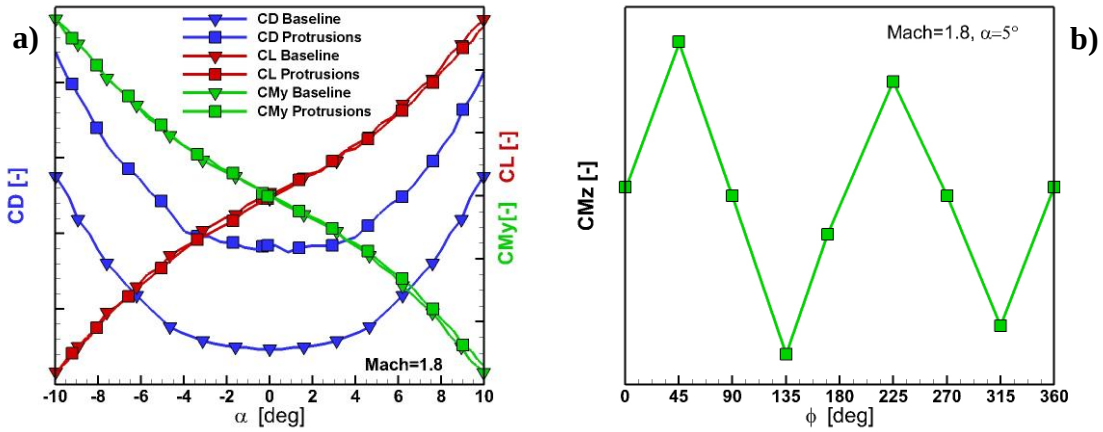

Figure 11: Protrusion effects am M=1.8: a) CD, CL and CMy vs α, b) CMz vs ϕ at α=5°.

6 CONCLUDING REMARKS

An extensive numerical and experimental investigation was carried out in order to build up the Vega C aerodynamic database. A successful wind tunnel test campaign was performed at INCAS trisonic wind tunnel on a 1:30 scaled model integrated by a large number of numerical simulations to cover the complete range of atmospheric flight conditions. Main effect of the Reynolds, Mach, incidence angle, roll angle, protrusions on 3 and 4 stages configuration were addressed. Good agreement between numerical results and experimental measurements in wind tunnel conditions give confidence about the accuracy of data extrapolated in flight conditions.

7 ACKNOWLEDGEMENTS

C. Stoica, G. Stoican, G. Cojogaru and the whole technical staff of the INCAS Wind Tunnel are sincerely acknowledged for their effort and continuous support during the measurement campaign. The present activity is framed within a wider project aimed to build up the Vega C Aerodatabase.

REFERENCES

[1] Vega User's Manual, issue 4 rev.0, April 2014 <http://www.arianespace.com/wp-content/uploads/2015/09/Vega-Users-Manual_Issue-04_April-2014.pdf>

[2] V. Baudel. Vega C User's Manual, issue 0 rev.0, May 2018 < http://www.arianespace.com/wp-content/uploads/2018/07/Vega-C-user-manual-Issue-0-Revision-0_20180705.pdf>

[3] G.W. Jones, J.T. Jr Foughner "Investigation of buffet pressures on models of large manned launch vehicle configurations", NASA technical note D-1633, 1963.

[4] F. Munteanu, INCAS Trisonic Wind Tunnel, INCAS BULLETIN, (online) ISSN 2247–4528, (print) ISSN 2066–8201, ISSN–L 2066–8201, Vol.1, N.1, DOI: 10.13111/2066-8201.2009.1.1.2, pp. 5-11, 2009.

[5] P. Roncioni, P. L. Vitagliano, F. De Gregorio, F. Paglia, C. Milana. "Aerodatabase of Vega-C Launcher Development and Integration". Proceedings of *8th European Conference for Aeronautics and Space Sciences*, Madrid, Spain, (2019).

[6] P. Catalano, M. Amato. "An evaluation of RANS turbulence modelling for aerodynamics applications", *Aerospace Science and Technology*, **7**, pp. 493-509, (2003).

[7] C. Marongiu, P. Catalano, M. Amato, G. Iaccarino. "U-ZEN: a computational tool solving U-RANS equations for industrial unsteady applications", Proceedings of *34th AIAA Fluid Dynamics Conference*, Portland, OR, USA, (2004).

[8] A. Nicolì, B. Imperatore, M. Marini, P. Catalano, A. Pizzicaroli and D. Perego. Ground-to-Flight Extrapolation of the Aerodynamic Coefficients of the VEGA Launcher. Proceedings of *25th AIAA Aerodynamic Measurement Technology and Ground Testing Conference*, San Francisco, California, (2006).

[9] P. Catalano, M. Marini, A. Nicolì, A. Pizzicaroli. CFD Contribution to the Aerodynamic Data Set of the Vega Launcher. *Journal of Spacecraft and Rockets* 44: 42-51, (2007).

[10] Ranuzzi G., D. Cardillo, M. Invigorito "Numerical Investigation of a N2O-Paraffin Hybrid Rocket Engine Combusting Flowfield", Proceedings of *6th European Conference For Aeronautics And Space Sciences*, (2015).